Three-Dimensional Simulation of Coherent Inverse Compton Scattering

by

Giacomo Rosario Resta

Submitted to the Department of Physics
in partial fulfillment of the requirements for the degree of

BACHELOR OF SCIENCE

at the

MASSACHUSETTS INSTITUTE OF TECHNOLOGY

June 2014

Signature redacted

Author ....
Department of Physics
May 18, 2014

Signature redacted

Certified by .....
David E. Moncton
Adjunct Professor of Physics, Department of Physics
Thesis Supervisor

Signature redacted

Certified by ....
William S. Graves
Principal Research Scientist, Nuclear Reactor Laboratory
Thesis Co-Supervisor

Signature redacted

Accepted by ....
Nergis Mavalvala
Senior Thesis Coordinator, Department of Physics

Three-Dimensional Simulation of Coherent Inverse Compton Scattering

by

Giacomo Rosario Resta

Submitted to the Department of Physics
on May 18, 2014, in partial fulfillment of the
requirements for the degree of
BACHELOR OF SCIENCE

Abstract

Novel compact X-ray sources using coherent ICS have the potential to positively impact a wide range of sectors by making hard x-ray techniques more accessible. However, the analysis of such novel sources requires improvements to existing simulation routines to incorporate Coulomb forces among particles and effects related to the phase of emitted radiation. This thesis develops a numerical routine for calculating the radiation scattered by electrons counter-propagating with a linearly-polarized, Gaussian laser pulse. The routine takes into account electron-electron repulsion and the constructive and destructive interference between the radiation emitted by each electron, making it suitable for characterizing the properties of inverse Compton scattering (ICS) sources where the electron density varies on the order of the laser wavelength. Finally, an analysis of the emission characteristics for an example ICS source with coherent emission at 10 nm wavelength is included. The source uses a 2 MeV electron bunch and a 1 μm wavelength laser. The coherent emission demonstrates a significantly narrowed linewidth and greatly increased output power when compared to traditional ICS.

Thesis Supervisor: David E. Moncton
Title: Adjunct Professor of Physics, Department of Physics

Thesis Co-Supervisor: William S. Graves
Title: Principal Research Scientist, Nuclear Reactor Laboratory

Acknowledgments

I would like to thank Boris Khaykovich, Bill Graves and David Moncton for allowing me to research within their group throughout my undergraduate studies.

Likewise, I would like to thank my parents: Franca and Giulio Resta, for their support and encouragement over these past four years.

Contents

List of Figures

List of Tables

Notation

Three-dimensional vectors are denoted with an arrow on top: $\vec{v}, \vec{x}, \ldots$
Four-dimensional vectors are denoted in bold: $\mathbf{p}, \mathbf{r}, \ldots$
A metric with the signature $(- + ++)$ is used, mainly,

$$\eta = \begin{bmatrix} -1 & 0 & 0 & 0 \\ 0 & 1 & 0 & 0 \\ 0 & 0 & 1 & 0 \\ 0 & 0 & 0 & 1 \end{bmatrix}.$$

Permittivity of free-space: ϵ_0
Speed of light in vacuum: c
Angular-frequency: ω
Transpose of a tensor is denoted by a super-script T (eg. $\mathbf{p}^T$).

Chapter 1

Introduction

Today x-rays provide an indispensable tool for analyzing the structure of matter in a wide area of applications from medical imaging, to the inspection of industrial components, to a number of uses in the physical, chemical and biological sciences. While many of these applications are only made possible thanks to the versatility of conventional or rotating-anode-based x-ray sources, improved flux and brilliance is in great demand for the hard x-ray regime. Current methods for generating hard x-rays, such as synchrotrons and free-electron lasers (FELs), require large storage rings or long ($\sim$ 1 km) linear accelerators. As a result, the prohibitively large and expensive nature of such sources limits the availability of a wide range of hard x-ray techniques.

The development of a compact source has the potential to enable modern x-ray science at institutions such as pharmaceutical companies and universities to accelerate analysis work which would currently require scheduling and sending samples to a distant facility.

Recently, a novel approach using coherent inverse Compton scattering (ICS) from electrons counter-propagating with an infrared laser may provide a less-expensive and more compact solution for generating x-ray beams comparable with 3rd generation synchrotrons [3]. The technique relies on using a nano-cathode field-emission array (FEA) to produce bundles of electrons spaced on the order of the x-ray wavelength.

While a large number of codes exist for simulating ICS and FEL interactions (PARMELA, GENESIS, ELEGANT, COMPTON, ...), these codes either assume that the phase of the radiation being emitted by each electron is uncorrelated, relying on approximations where the electron density varies over a characteristic length much larger than the laser wavelength or ignore the effects of Coulomb repulsion. As a result, such simulation codes are poorly suited for determining the emission properties for a coherent ICS source.

This thesis attempts to address the need for an ICS simulator which is able to track the phase of the radiation emitted by each electron, and take into account effects due to electron-electron repulsion. In doing so, it attempts to provide an additional tool to facilitate the design and analysis of such ICS sources currently under consideration.

1.1 Overview of ICS for Hard X-ray Generation

There are two approaches within the literature for understanding the basic principle behind ICS sources, one from a Quantum-particle viewpoint and the other from the classical field theory of E&M.

For the quantum-particle standpoint, consider a relativistic collision between an electron

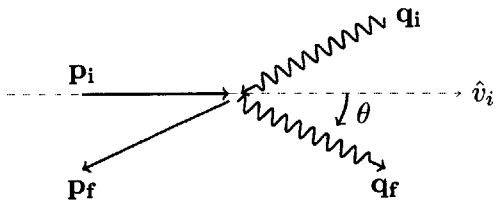

Figure 1-1: Illustration of an electron-photon collision along with the parameters used in the text. Note that θ is taken as the angle between the initial direction of travel of the electron and the direction of travel of the scattered photon. For a typical ICS setup, $\mathbf{p_f}$ points in the same direction as $\mathbf{p_i}$.

and a photon. Let $\mathbf{p_i}$ and $\mathbf{q_i}$ denote the initial four-vector momentum for the electron and photon respectively and $\mathbf{p_f}$ and $\mathbf{q_f}$ the final four-vector momentum. In terms of common parameters,

$$\mathbf{p_n} = \gamma_n m \left(c, \quad \vec{v}_n\right),$$
$$\mathbf{q_n} = \frac{\hbar\omega_n}{c}\left(1, \quad \hat{k}_n\right),$$

where ω_n and $\hat{k}_n$ are the angular-frequency and direction of travel of the photon, m and v_n are the mass and velocity of the electron and, γ_n is given by,

$$\gamma_n = \frac{1}{\sqrt{1 - \left(\frac{v_n}{c}\right)^2}}.$$

Using conservation of momentum,

$$\mathbf{p_f} + \mathbf{q_f} = \mathbf{p_i} + \mathbf{q_i},$$

we can determine an expression for the final momentum of the electron, mainly,

$$\mathbf{p_f} = \mathbf{p_i} + \mathbf{q_i} - \mathbf{q_f}.$$

Taking the four-vector inner product of both sides of the above equation, and using the fact that, since $\eta = \eta^T$,

$$\begin{aligned}\mathbf{a}\cdot\eta\cdot\mathbf{b}^T &= \left(\mathbf{a}\cdot\eta\cdot\mathbf{b}^T\right)^T \\ &= \mathbf{b}\cdot\eta\cdot\mathbf{a}^T\end{aligned}$$

we find that,

$$\begin{aligned}\mathbf{p_f}\cdot\eta\cdot{\mathbf{p_f}}^T &= \left(\mathbf{p_i}+\mathbf{q_i}-\mathbf{q_f}\right)\cdot\eta\cdot\left(\mathbf{p_i}+\mathbf{q_i}-\mathbf{q_f}\right)^T \\ &= \mathbf{p_i}\cdot\eta\cdot{\mathbf{p_i}}^T + 2\mathbf{p_i}\cdot\eta\cdot{\mathbf{q_i}}^T - 2\mathbf{p_i}\cdot\eta\cdot{\mathbf{q_f}}^T - 2\mathbf{q_i}\cdot\eta\cdot{\mathbf{q_f}}^T + \mathbf{q_i}\cdot{\mathbf{q_i}}^T + \mathbf{q_f}\cdot{\mathbf{q_f}}^T.\end{aligned}$$

Using the definitions for $\mathbf{p}$ and $\mathbf{q}$ in terms of more common parameters and simplifying,

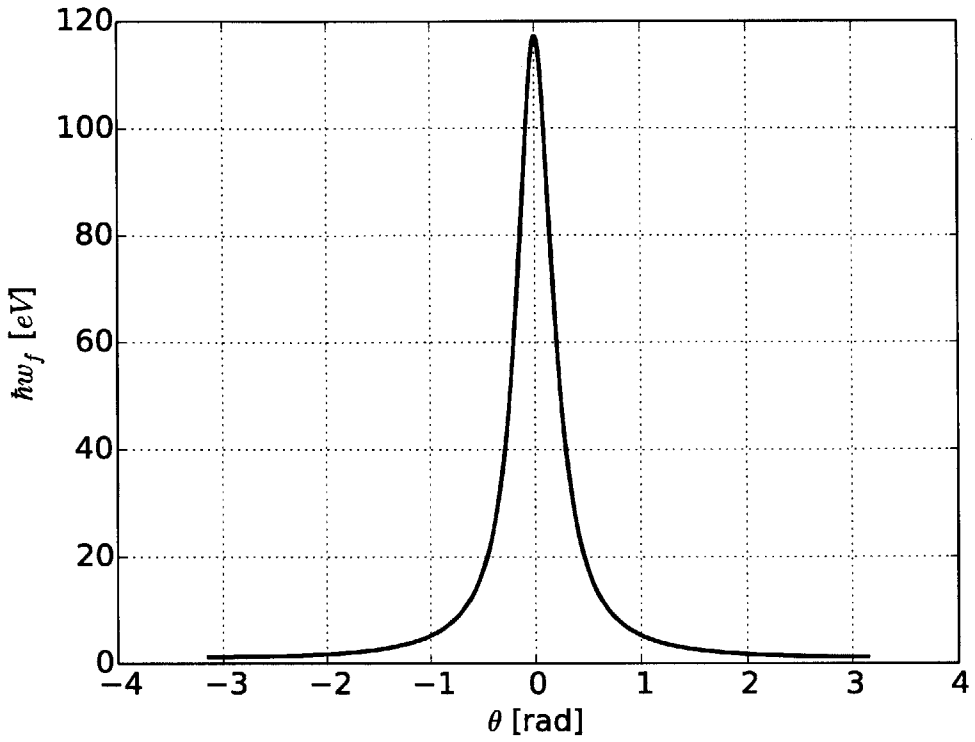

Figure 1-2: Plot of the energy of scattered photons by an electron for an electron kinetic energy of $E_k = 2 \times 10^6$ eV and laser wavelength of $\lambda = 10^{-6}$ m corresponding to an initial photon energy of 1.24 eV. The energy for scattered photons at $\theta = 0$ is 117 eV.

it is found that,

$$m^2c^2 = m^2c^2 - 2\gamma_i m\hbar\omega_i \left(\vec{v}_i \cdot \hat{k}_i - c\right) + 2\left(\gamma_i \left(\vec{v}_i \cdot \vec{k}_f - c\right) + \left(\vec{k}_i \cdot \vec{k}_f - 1\right)\frac{\hbar^2\omega_i}{c}\right)\omega_f,$$

which can be solved to determine the angular-frequency of the scattered photon ω_f,

$$\omega_f = \frac{\omega_i \left(c - \vec{v}_i \cdot \hat{k}_i\right)}{\left(c - \vec{v}_i \cdot \hat{k}_f\right) + \left(1 - \hat{k}_i \cdot \hat{k}_f\right)\frac{\hbar w_i}{\gamma_i mc}}. \tag{1.1}$$

Figure 1-2, plots the behavior of Equation 1.1 as a function of the angle θ between $\vec{v}_i$ and $\hat{k}_f$ for photon and electron energies of a sample ICS source. With the understanding that a laser consists of a distribution of photons, we can see that an electron counter-propagating with a laser will result in scattered photons propagating in the electron's direction with a much higher energy. It is this property of ICS that makes it suitable for the generation of hard X-rays.

1.2 Overview of Coherent ICS

To understand the effect periodic electron distributions have on the intensity emitted in coherent ICS, let us investigate the phenomena using Classical E&M in the non-relativistic limit where the electron velocity $v \ll c$.

Consider a linearly-polarized plane-wave propagating in the negative $\hat{z}$ direction. Letting,

$$\begin{aligned}\phi &= z + ct,\\ E &= E_0 \cos(k\phi),\\ \hat{k} &= -\hat{z},\end{aligned}$$

the E&M fields of the plane-wave are given by,

$$\vec{E} = E\hat{y}, \tag{1.2}$$

$$\vec{B} = \frac{1}{c}\hat{k} \times \vec{E} = \frac{E}{c}\hat{x}. \tag{1.3}$$

Let $\vec{r}$ denote the position of an electron. Using the Lorentz force equation,

$$\vec{F} = q\left(\vec{E} + \dot{\vec{r}} \times \vec{B}\right), \tag{1.4}$$

the non-relativistic equations of motion can be readily found,

$$\begin{aligned}\ddot{r}_x &= 0\\ \ddot{r}_y &= \frac{qE}{m}\left(1 + \frac{\dot{r}_z}{c}\right)\\ \ddot{r}_z &= -\frac{qE}{m}\frac{\dot{r}_y}{c}\end{aligned}$$

Since we assume that the electron velocity $v \ll c$, we can ignore terms of the form $\dot{r}_i/c$ in the above equations, reducing them to,

$$\begin{aligned}\ddot{r}_x &= 0,\\ \ddot{r}_y &= \frac{qE}{m} = \frac{qE_0}{m}\cos(k\,(r_z + ct)),\\ \ddot{r}_z &= 0,\end{aligned}$$

which can be easily integrated by noting that,

$$\begin{aligned}r_x &= v_x t + x_0,\\ r_z &= v_z t + z_0,\end{aligned}$$

and hence,

$$\ddot{r}_y = \frac{qE_0}{m}\cos(k\,((v_z + c)t + z_0)), \tag{1.5}$$

$$r_y = -\frac{qE_0}{mk^2(v_z + c)^2}\cos\left(k((v_z + c)t) + kz_0\right) + v_y t + y_0. \tag{1.6}$$

To simplify calculating the radiation emitted, let us assume that the motion of the electrons deviate slightly from a ballistic trajectory along the z-axis,

$$\vec{r}(t) \cong (v_z t + z_0)\hat{z}.$$

This requires that $v_x = v_y = x_0 = y_0 = 0$ and, that the oscillatory term in the equation for r_y is relatively small compared to the distance at which the system is being observed. This last requirement essentially places a constraint on the strength of the plane-wave.

Letting $\vec{R}$ denote the point where the radiation will be observed, the radiation from a non-relativistic charge is then given by,

$$\vec{E}_{rad} = \frac{q}{4\pi\epsilon_0 c^2 |\vec{n}|}\left(\ddot{\vec{r}}(t_r) \times \hat{n}\right) \times \hat{n},$$

where,

$$\vec{n} = \vec{R} - \vec{r}(t_r),$$
$$t_r = t - \frac{|\vec{n}|}{c}.$$

If we let the observation point be on the z-axis such that $\vec{R} = R_0\hat{z}$, we can simplify the equation for the radiation to,

$$\vec{E}_{rad} = \frac{q}{4\pi\epsilon_0 c^2 n}\left(\ddot{\vec{r}}(t_r) \times \hat{z}\right) \times \hat{z},$$

where,

$$n = R_0 - v_z t_r - z_0,$$
$$t_r = t - \frac{R_0}{c} + \frac{v_z t_r + z_0}{c},$$
$$= \frac{ct - R_0 + z_0}{c - v_z}.$$

Finally, let us assume that the electrons are localized in a region of space of length $l = \Delta z_0$, such that $\Delta z_0 \ll R_0$. We note that the difference in t_r for each of the electrons is given by,

$$\Delta t_r = \frac{\Delta z_0}{c - v_z},$$
$$\cong \frac{\Delta z_0}{c}.$$

and hence, it follows that,

$$v_z \Delta t_r \ll R_0.$$

Likewise, let us sample around the time,

$$t = \frac{R_0}{c} + t',$$

where ct' is on the order of the laser wavelength.

With these requirements, the equation for the radiation simplifies to,

$$\vec{E}_{rad} = \frac{q}{4\pi\epsilon_0 c^2 R_0}\left(\ddot{\vec{r}}(t_r) \times \hat{z}\right) \times \hat{z}, \tag{1.7}$$

where,

$$t_r = \frac{ct' + z_0}{c - v_z}.$$

Combining Equations 1.5 and 1.7, we find that the electron radiation is given by,

$$\vec{E}_{rad} = -\frac{q^2 E_0}{4\pi\epsilon_0 mc^2 R_0} \cos\left(\frac{ck(v_z + c)}{(c - v_z)}t' + k\left(\frac{v_z + c}{c - v_z} + 1\right) z_0\right) \hat{y}.$$

Switching to complex notation,

$$\vec{E}_{rad} = -\frac{q^2 E_0}{4\pi\epsilon_0 mc^2 R_0} \exp\left(ik\left(\frac{2c}{c - v_z}\right) z_0\right) \exp\left(i\frac{ck(v_z + c)}{(c - v_z)}t'\right) \hat{y}.$$

We make one immediate observation, mainly that the angular-frequency of the emitted radiation ω_s is given by,

$$\omega_s = \frac{(v_z + c)\omega_i}{c - v_z},$$

where we have used the relation $\omega_i = ck$. This is consistent with Equation 1.1, when noting that for this setup $\hat{k}_i = -\hat{z}$ and $\hat{k}_f = \hat{z}$ and, the necessary classical limit $\hbar\omega_i \ll \gamma mc^2$ is respected.

We can now analyze the effects the spatial distribution of an electron pulse has on the radiation emitted. Consider a line of electrons situated at the origin with a length l much larger than the period of the radiation, but as required by the above derivation $l \ll R_0$. Let $\rho(z)$ denote the density of electrons as a function of z such that,

$$N_e = \int_{-l/2}^{l/2} \rho(z)dz,$$

where N_e is the total number of electrons in the pulse. The electric-field at observation point $\vec{R}$ is then given by,

$$\vec{E}_{rad} = -\frac{q^2 E_0}{4\pi\epsilon_0 mc^2 R_0}\left[\int_{-l/2}^{l/2} \exp\left(ik\left(\frac{2c}{c - v_z}\right) z\right) \rho(z)dz\right] \exp\left(i\frac{ck(v_z + c)}{(c - v_z)}t'\right) \hat{y}. \tag{1.8}$$

Two particular forms for $\rho(z)$ are of interest. The first is a Gaussian distribution well contained between $-l/2$ and $l/2$, for instance,

$$\rho_{nc}(z) = \frac{N_e}{\sigma\sqrt{2\pi}} \exp\left(-\frac{z^2}{2\sigma^2}\right),$$

where we let $\sigma = l/8$. Figure 1-3 plots this distribution, demonstrating that it is well-contained between $-l/2$ and $l/2$.

Since the density is well contained, we find a good approximation to evaluating Equation 1.8 using the density ρ_{nc} by approximating the integral as being over the range

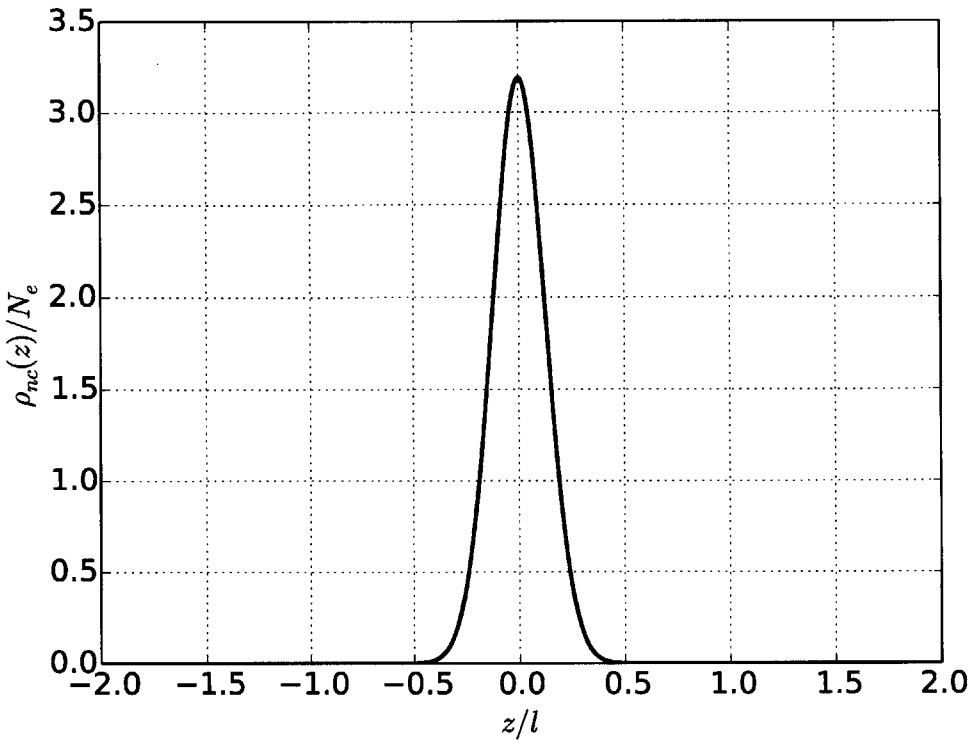

Figure 1-3: Plot of Gaussian electron density distribution. Note that the distribution is well contained within the range $-l/2$ to $l/2$.

$(-\infty, \infty)$. Doing so, we find that,

$$\vec{E}_{nc} = -\frac{q^2 E_0}{4\pi\epsilon_0 mc^2 R_0} N_e \exp\left(-\frac{1}{2}\left(k\frac{c}{(c-v_z)}\frac{l}{8}\right)^2\right) \exp\left(i\frac{ck(v_z+c)}{(c-v_z)}t'\right)\hat{y}.$$

Computing the time-average intensity,

$$\langle I_{nc}\rangle = \frac{\epsilon_0 c}{2}|\vec{E}_{nc}|^2, \tag{1.9}$$

$$= \frac{q^4 E_0^2 N_e^2}{32\pi^2\epsilon_0 mc^3 R_0^2} \exp\left(-\left(k\frac{2c}{(c-v_z)}\frac{l}{8}\right)^2\right). \tag{1.10}$$

The second functional form of interest is a distribution where electrons are separated by a distance,

$$\Delta z = \lambda\frac{(c-v_z)}{2c}, \tag{1.11}$$

where λ is the wavelength of the plane-wave. Letting m be an integer such that $0 < m < l/\Delta z$, this distribution is given by,

$$\rho_c(z) = \sum_{a=0}^{m} \frac{N_e}{m+1}\delta\left(\left(\frac{l}{2} - a\Delta z\right) - z\right),$$

where δ denotes the dirac-delta function. Evaluating Equation 1.8 using the density ρ_c is

simple,

$$\vec{E_c} = -\frac{q^2 E_0}{4\pi\epsilon_0 mc^2 R_0}\left[\int_{-l/2}^{l/2} \exp\left(ik\left(\frac{2c}{c-v_z}\right)z\right)\sum_{a=0}^{m}\frac{N_e}{m+1}\delta\left(\left(\frac{l}{2}-a\Delta z\right)-z\right)dz\right]\exp\left(i\frac{ck(v_z+c)}{(c-v_z)}t'\right)\hat{y}$$
$$= -\frac{q^2 E_0}{4\pi\epsilon_0 mc^2 R_0}N_e \exp\left(i\frac{2\pi}{\Delta z}\frac{l}{2}\right)\exp\left(i\frac{ck(v_z+c)}{(c-v_z)}t'\right)\hat{y}.$$

Computing the time-average intensity, we find,

$$\langle I_c\rangle = \frac{q^4 E_0^2 N_e^2}{32\pi^2\epsilon_0 m^2 c^3 R_0^2}. \tag{1.12}$$

(1.13)

Comparing I_c above to Equation 1.10, we see that the exponential representing partial constructive interference is missing, resulting in a much higher intensity for the coherent case.

1.3 Outline of Thesis

While the arguments above are useful for illustrating the general concept behind a coherent ICS source, a rigorous analysis taking into account additional factors such as space-charge effects and the relativistic motion of electrons within a laser beam requires a numerical simulation routine.

Chapter 2 follows a similar structure as Section 1.2 but in a more rigorous fashion. Two realistic models for a laser pulse with a Gaussian energy distribution are discussed, the radiation scattered by a relativistic electron is considered and finally, a method for introducing space-charge forces is presented.

Chapter 3 discusses two numerical methods used within the software to implement the routine discussed in Chapter 2. One of the methods is related to accelerating the computation of space-charge forces on each electron by using an Octree, where as the other method is related to how the equations of motion are integrated.

In Chapter 4, parameters for an example ICS source are analyzed. Both the energy and spatial profile of the emitted beam as well as the dependency of the beam profile on the spacing between the electron bunches is discussed for both a coherently and incoherently radiating electron density.

Chapter 2

Classical E&M Derivation for ICS

To incorporate effects due to the phase of scattered radiation into our simulations, we have selected to follow a derivation of ICS from the standpoint of classical E&M. The validity of Classical E&M in analyzing the radiation from an electron assumes that the energy of the electron is much greater than that of the incident photon [8],

$$\hbar\omega \ll \gamma mc^2. \tag{2.1}$$

For the electron and photon energies under consideration this approximation is well justified.

2.1 The Gaussian Plane-Wave Laser Pulse

We begin by considering a simple model for a linearly-polarized Gaussian laser pulse as consisting of a Gaussian distribution of energies in the plane-wave propagation mode. Let us introduce the forward Fourier Transformation,

$$\widetilde{f}(\omega) = \int_{-\infty}^{\infty} f(t)e^{-i\omega t}dt, \tag{2.2}$$

and inverse Fourier Transformation,

$$f(t) = \frac{1}{2\pi}\int_{-\infty}^{\infty} \widetilde{f}(\omega)e^{i\omega t}d\omega. \tag{2.3}$$

Consider the electric field of a simple monochromatic plane-wave of angular-frequency w_0, traveling in the $-\hat{z}$ direction,

$$E(z,t)_{mpw} = E_0 \exp\left(i\omega_0\left(t+\frac{z}{c}\right)\right) + c.c.$$

Using the inverse Fourier Transformation, we find that the representation for this field in frequency-domain is given by,

$$\widetilde{E}_{mpw}(\omega) = E_0 \exp\left(i\omega\frac{z}{c}\right) 2\pi\delta(\omega_0-\omega),$$

From this frequency-domain representation of a mono-chromatic plane-wave, we can identify that part of the expression is related to the amplitude of the plane-wave propagation

mode and the other part is related to the normalized energy spectrum,

$$\widetilde{E}_{mpw}(\omega) = \underbrace{E_0 \exp\left(i\omega\frac{z}{c}\right)}_{\text{freq.-domain plane-wave amplitude}} \underbrace{2\pi\delta(\omega_0 - \omega)}_{\text{energy spectrum}}.$$

The E-field of a mono-chromatic plane-wave can therefore be understood as the inverse Fourier transformation of the product of the frequency-domain amplitude of the plane-wave mode ($\widetilde{E}_{pw}$) with the mono-chromatic energy spectrum ($\widetilde{F}_{mc}$),

$$E_{mpw}(z,t) = \frac{1}{2\pi}\int_{-\infty}^{\infty} \widetilde{E}_{pw}(\omega)\widetilde{F}_{mc}(\omega)e^{i\omega t}d\omega, \tag{2.4}$$

where,

$$\widetilde{E}_{pw}(z,\omega) = E_0 \exp\left(i\omega\frac{z}{c}\right), \tag{2.5}$$

$$\widetilde{F}_{mc}(\omega) = 2\pi\delta(\omega_0 - \omega). \tag{2.6}$$

To determine an expression for a plane-wave with a Gaussian energy distribution, we introduce the energy distribution [11],

$$\widetilde{F}_g(\omega) = \sqrt{\frac{\pi}{p}} \exp\left(-\frac{(\omega-\omega_0)^2}{4p}\right), \tag{2.7}$$

where p is a parameter related to the width of the distribution.

The electric field of the Gaussian plane-wave pulse can then be determined with the following,

$$E_{gpw}(z,t) = \frac{1}{2\pi}\int_{-\infty}^{\infty} \widetilde{E}_{pw}(\omega)\widetilde{F}_g(\omega)e^{i\omega t}d\omega$$

$$E_{gpw}(z,t) = E_0 \exp\left(-p\left(t+\frac{z}{c}\right)^2\right)\exp\left(i\omega_0\left(t+\frac{z}{c}\right)\right) \tag{2.8}$$

From the above equation, we note that the $1/e$ width of the pulse (ct_0) is related to the energy distribution parameter p by,

$$p = \left(\frac{c}{ct_0}\right)^2.$$

As a result, we find that the representation for the electric-field of a Gaussian modulated plane-wave is given by,

$$\widetilde{E}_{gpw}(z,\omega) = E_0 t_0\sqrt{\pi}\exp\left(-\frac{(\omega-\omega_0)^2 t_0^2}{4}\right)\exp\left(i\omega\frac{z}{c}\right), \tag{2.9}$$

$$E_{gpw}(z,t) = E_0 \exp\left(\frac{(ct+z)^2}{c^2 t_0^2}\right)\exp\left(i\frac{\omega_0}{c}(ct+z)\right). \tag{2.10}$$

We note that in the limit where the $1/e$ pulse length is much larger than the wavelength

corresponding to w_0,

$$\frac{2\pi c}{w_0} \ll ct_0,$$

the second exponential term in Equation 2.10 results in a rapid oscillation compared to the first exponential which is responsible for a slow modulation of the amplitude,

$$E_{gpw}(z,t) = E_0 \underbrace{\exp\left(\frac{(ct+z)^2}{c^2 t_0^2}\right)}_{\text{Slow Amplitude Modulation}} \underbrace{\exp\left(i\frac{\omega_0}{c}(ct+z)\right)}_{\text{Rapid oscillation}}.$$

2.2 The Gaussian Beam Laser Pulse

The above equation for a Gaussian plane-wave is suitable for modeling situations in which the electron bunch is transversely spread over a region of the laser where the profile is relatively constant. However, if the transverse electron bunch size is comparable to the transverse profile of the laser, a more accurate model which likewise encapsulates the transverse Gaussian-like modulation of the laser is required. To determine such a representation, we can perform a similar derivation as in Section 2.1, however using the Gaussian beam mode instead of the plane-wave propagation mode.

The amplitude for a Gaussian beam along $-\hat{z}$ in frequency-domain representation is given by [11],

$$\widetilde{E}_g(r,z,\omega) = E_0 \frac{w_0}{w(z)} \exp\left(-\frac{r^2}{w(z)^2} - i\eta + ikz + \frac{ikr^2}{2R(z)}\right), \tag{2.11}$$

where,

$$r = \sqrt{x^2+y^2},$$

$$\text{Beam Waist} \rightarrow w(z) = w_0\sqrt{1+\left(\frac{z}{z_0}\right)^2},$$

$$\text{Radius of Curvature} \rightarrow R(z) = z\left(1+\left(\frac{z_0}{z}\right)^2\right),$$

$$\text{Gouy Phase} \rightarrow \eta(z) = \arctan\left(\frac{z}{z_0}\right),$$

$$\text{Diffraction Length} \rightarrow z_0 = \frac{\pi w_0^2}{\lambda},$$

$$\text{Wave Number} \rightarrow k_0 = \frac{\omega}{c}.$$

By again using a Gaussian energy modulation [11],

$$\widetilde{F}(\omega) = \sqrt{\frac{\pi}{p}} \exp\left(-\frac{(\omega-\omega_0)^2}{4p}\right),$$

the expression for the Gaussian pulse is given by,

$$E(r,z,t)_{gg} = \frac{1}{2\pi}\int_{-\infty}^{\infty} \widetilde{E}_g(r,z,\omega)\widetilde{F}_g(\omega)e^{i\omega t}d\omega.$$

Determining an analytic expression for the above integral is difficult if we assume that the waist size is independent of the wave number [11]. However, in the case of a confocal resonator, the waist size depends on the wave number according to [9],

$$w_0 = \sqrt{\frac{L}{k}},$$

where L is the length of the resonator.

Under these circumstances an analytic expression can be easily derived [10]. The field for a Gaussian Beam pulse is given by,

$$E(r,z,t)_{gg} = E_0 m(z)\exp\left(-\left(\frac{\tau}{ct_0}\right)^2 + ik_0\tau - i\eta(z)\right), \tag{2.12}$$

where ct_0 is the $1/e$ length of pulse and,

$$\begin{aligned}
\tau &= \frac{ir^2m(z)^2}{L} + \frac{r^2}{2}q(z) + z + ct,\\
\text{Gouy Phase} \rightarrow \eta(z) &= \arctan\left(\frac{z}{z_0}\right),\\
m(z) &= \left(1+\left(\frac{z}{z_0}\right)^2\right)^{-1/2},\\
q(z) &= \frac{z}{z^2+z_0^2},\\
\text{Diffraction Length} \rightarrow z_0 &= \frac{L}{2},\\
\text{Length of resonator cavity} \rightarrow L &= w_0^2 k_0.
\end{aligned}$$

We can rewrite Equation 2.12 to better illustrate the nature of the pulse. Letting,

$$\phi = ct + z,$$

we note that,

$$E(r,z,t)_{gg} = \underbrace{E_0 m(z) \exp\left(-\frac{1}{(ct_0)^2}\left(\frac{r^4}{4}q^2(z) - \frac{r^4 m(z)^4}{L^2} + r^2 q(z)\phi + \phi^2\right)\right)}_{\text{Amplitude modulation}}$$
$$\underbrace{\times \exp\left(-i\left(\frac{r^4 m(z)^2 q(z)}{2L(ct_0)^2} + \eta(z)\right)\right)}_{\text{Phase modulation}}$$
$$\underbrace{\times \exp\left(i\left(k_0 - \frac{2r^2 m(z)^2}{L(ct_0)^2}\right)\phi\right)}_{\text{Fast oscillation}}.$$

2.3 Derivation of the Equations of Motion for Plane-Wave Approximation

We can determine an approximate relation for the radiation scattered by an electron by considering its motion within a monochromatic plane-wave. We begin with a general derivation of the relativistic equations of motion for a single electron counter-propagating with a linearly polarized plane-wave in the negative $\hat{z}$ direction [7] [5].

Letting,

$$\phi = z + ct,$$
$$E = E_0 \cos(k\phi + \delta_1),$$

the E&M fields for a plane-wave traveling in the $\hat{k} = -\hat{z}$ and linearly polarized in the $\hat{y}$ direction are given by,

$$\vec{E} = E\hat{y},$$
$$\vec{B} = \frac{1}{c}\hat{k} \times \vec{E} = \frac{E}{c}\hat{x}.$$

Using the Lorentz force law,

$$\frac{d\vec{p}}{dt} = q\left(\vec{E} + \dot{\vec{r}} \times \vec{B}\right), \tag{2.13}$$

the equations of motion can be easily determined, mainly,

$$\frac{dp_x}{dt} = 0,$$
$$\frac{dp_y}{dt} = q\left(1 + \frac{\dot{r}_z}{c}\right)E,$$
$$\frac{dp_z}{dt} = -qE\dot{r}_y.$$

From the above, we note that p_x is a constant of motion $p_x = p_{x0}$. Likewise, the equation for p_y can be easily integrated since,

$$\frac{d\phi}{dt} = c + \dot{r}_z.$$

Hence,

$$\frac{d\phi}{dt}\frac{dp_y}{d\phi} = q\left(1+\frac{\dot{r}_z}{c}\right)E,$$
$$p_y = \frac{qE_0}{ck}\sin\left(k\phi+\delta_1\right)+c_2. \tag{2.14}$$

Noting that the total energy of the particle is given by $E=\gamma mc^2$ and that,

$$\frac{dE}{dt} = \dot{\vec{r}}\cdot\frac{d\vec{p}}{dt},$$
$$\frac{d(\gamma mc^2)}{dt} = \dot{\vec{r}}\cdot\left(qE+\dot{\vec{r}}\times\vec{B}\right),$$

using the fact that $\dot{\vec{r}}\cdot\left(\dot{\vec{r}}\times\vec{B}\right)=0$,

$$\frac{d(\gamma mc^2)}{dt} = q\dot{\vec{r}}\cdot\vec{E},$$
$$= q\dot{r}_y E,$$

a simple expression for the derivative of γ can be determined,

$$\frac{d\gamma}{dt} = \frac{q\dot{r}_y E}{mc^2}. \tag{2.15}$$

Solving for $\dot{r}_y$ in the above expression, and substituting it into the derivative for p_z, we find,

$$\frac{dp_z}{dt} = -\frac{d\gamma}{dt}mc,$$

and hence,

$$p_z = c_1-\gamma mc,$$

where c_1 is a constant of integration.

Finally, using the fact that the inner product of the four-momentum is given by,

$$-m^2c^2 = \mathbf{p}\cdot\eta\cdot\mathbf{p}^T,$$
$$-m^2c^2 = -\gamma^2m^2c^2+p_x^2+p_y^2+p_z^2.$$

and plugging in our determined expressions for p_x, p_y and p_z, we find that,

$$-m^2c^2 = -\gamma^2m^2c^2+p_{x0}^2+p_y^2+c_1^2-2\gamma mcc_1+\gamma^2m^2c^2,$$
$$-m^2c^2 = p_{x0}^2+p_y^2+c_1^2-2\gamma mcc_1,$$

solving for γ,

$$\gamma = \frac{m^2c^2+p_x^2+p_y^2+c_1^2}{2mcc_1}. \tag{2.16}$$

We note that the expression for the momentum of the electron are trivial to integrate with respect to ϕ, since,

$$\begin{aligned}\frac{d\phi}{dt} &= c + \dot{r}_z, = c + \frac{p_z}{\gamma m},\\ &= \frac{c_1}{\gamma m}.\end{aligned}$$

Therefore, using,

$$\begin{aligned}\frac{d\vec{r}}{dt} &= \frac{\vec{p}}{\gamma m},\\ \frac{d\phi}{dt}\frac{d\vec{r}}{d\phi} &= \frac{\vec{p}}{\gamma m},\\ \frac{d\vec{r}}{d\phi} &= \frac{\vec{p}}{c_1},\end{aligned}$$

an expression for the position of the electron can be easily determined,

$$r_x = \frac{p_x}{c_1}\phi + c_3, \tag{2.17}$$

$$r_y = \frac{1}{c_1}\left(-\frac{qE_0}{ck^2}\cos(k\phi + \delta_1) + c_2\phi\right) + c_4, \tag{2.18}$$

$$\begin{aligned}r_z = \frac{1}{2c_1^2}\Bigg(&\left(\frac{qE_0}{ck}\right)^2\frac{1}{4k}\sin(2k\phi + 2\delta_1) + 2c_2\frac{qE_0}{ck^2}\cos(k\phi + \delta_1)\\ &- \left(m^2c^2 + p_x^2 - c_1^2 + c_2^2 + \left(\frac{qE_0}{ck}\right)^2\frac{1}{2}\right)\phi\Bigg) + c_5.\end{aligned} \tag{2.19}$$

2.4 Calculating Scattered Radiation

The electric field for a point charge in arbitrary motion is given by [4],

$$\vec{E}(\vec{R},t) = \frac{q}{4\pi\epsilon_0}\frac{|\vec{x}|}{(\vec{x}\cdot\vec{u})^3}\left[(c^2 - v^2)\vec{u} + \vec{x}\times(\vec{u}\times\vec{a})\right] \tag{2.20}$$

$$\vec{B}(\vec{R},t) = \frac{1}{c}\vec{x}\times\vec{E}(\vec{R},t) \tag{2.21}$$

where,

$$\begin{aligned}\text{Position of particle} &\rightarrow \vec{r}(t_r)\\ \text{Velocity of particle} &\rightarrow \vec{v} = \dot{\vec{r}}(t_r)\\ \text{Acceleration of particle} &\rightarrow \vec{a} = \ddot{\vec{r}}(t_r)\\ \text{Observation point} &\rightarrow \vec{R}\\ \text{Vector from emission to observation point} &\rightarrow \vec{x} = \vec{R} - \vec{r}(t_r)\\ \text{Retarded time} &\rightarrow t_r = t - \frac{|\vec{x}|}{c}\\ &\vec{u} = c\hat{x} - \vec{v}\end{aligned}$$

However, since only terms which scale like $1/|x|$ propagate to infinity, the radiation from a point charge in arbitrary motion is given by,

$$\vec{E}_{rad}(\vec{R},t) = \frac{q}{4\pi\epsilon_0}\frac{|\vec{x}|}{(\vec{x}\cdot\vec{u})^3}\left[\vec{x}\times(\vec{u}\times\vec{a})\right], \tag{2.22}$$
$$\vec{B}(\vec{R},t) = \frac{1}{c}\vec{x}\times\vec{E}(\vec{R},t).$$

To determine the acceleration vector $\vec{a}$ we note that,

$$\vec{a} = \frac{d\vec{v}}{dt} = \frac{d}{dt}\left(\frac{\vec{p}}{\gamma m}\right) = \frac{1}{\gamma m}\frac{d\vec{p}}{dt} + \frac{\vec{p}}{m}\frac{d\gamma}{dt}.$$

Using the expressions derived in Section 2.3 for $\vec{p}$, $d\gamma/dt$ and, $d\vec{p}/dt$, we find that,

$$\vec{a} = \begin{pmatrix} -\frac{qp_yp_x}{\gamma^3m^3c^2}E_0\cos(k\phi+\delta_1) \\ \frac{q}{\gamma^2m^2c}E_0\cos(k\phi+\delta_1)\left(c_1 - \frac{p_y^2}{\gamma mc}\right) \\ -\frac{qp_yc_1}{\gamma^3m^3c^2}E_0\cos(k\phi+\delta_1) \end{pmatrix}. \tag{2.23}$$

2.5 Sampling Radiation from Multiple Electrons

While the exact electric field from a single electron can be easily determined using Equation 2.22 in conjunction with the derived expressions for the motion of the electron, summing the radiation from multiple electrons using such an exact approach is complicated by the fact that the expressions for the equation of motion are a function of ϕ, while the electric field must be summed with respect to time. Methods explored to overcome this difficulty while introducing no additional approximations proved to be too computationally intensive or unreliable, especially since many quantities of interest (such as intensity) are time average values of the electric field. However, we can introduce two reasonable approximations that simplify the problem.

First, we approximate the motion of the electron as being ballistic as it traverses one wavelength of the laser. From Equations 2.14 we can see that if,

$$\frac{qE_0}{ck} \ll |\vec{p}|,$$

then the oscillations in the y component of the momentum are relatively small compared to the total momentum of the electron. As a result, we can consider the electron as effectively having a constant velocity $\vec{v}(t_0)$ as it traverses one wavelength of the laser, such that,

$$\vec{r}(t_r) \cong \vec{v}(t_0)(t_r - t_0) + \vec{r}(t_0) \tag{2.24}$$

and,

$$\gamma(t_r) \cong \gamma(t_0),$$

is approximately constant. Under this ballistic assumption we can rewrite Equation 2.23

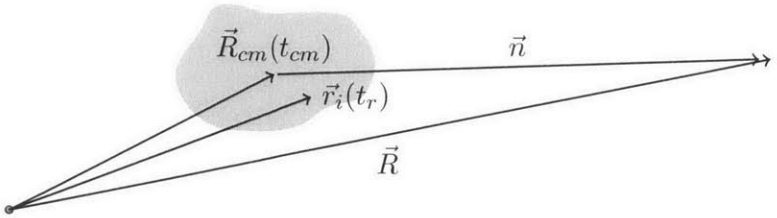

Figure 2-1: Illustration of the vectors used in the far field approximation. The gray polygon represents the electron distribution, $\vec{R}_{cm}(t_{cm})$ is the center of mass of the electron distribution, $\vec{r}_i(t_r)$ is the location of the i^{th} electron, and $\vec{R}$ is the observation point.

as,

$$\vec{a} = \frac{qE_0}{m} \cos\left(k\phi + \delta_1\right) \vec{g} \tag{2.25}$$

where,

$$\vec{g} = \frac{1}{\gamma c^2} \left(-v_x v_y, \quad cv_z + c^2 - v_y^2, \quad v_y(v_z + c)\right). \tag{2.26}$$

Using Equation 2.22 we now see that the electric field is given by an equation with the form of a plane-wave,

$$\vec{E}_{rad}(\vec{r}, t) = \underbrace{\frac{q^2 E_0}{4\pi\epsilon_0 m} \frac{|\vec{x}|}{(c|\vec{x}| - \vec{x}\cdot\vec{v})^3} \left[\vec{x} \times ((c\hat{x} - \vec{v}) \times \vec{g})\right]}_{\text{Amplitude}} \underbrace{\cos\left(k\phi + \delta_1\right)}_{\text{Oscillating Term}}, \tag{2.27}$$

which has a quasi-periodic value within the interval,

$$\Delta\phi = \frac{2\pi}{k}. \tag{2.28}$$

From the definition for ϕ, and using Equation 2.24 we see that,

$$\Delta\phi = c\Delta t_r + \Delta z, \tag{2.29}$$

$$= (c + \vec{v}\cdot\hat{z})\Delta t_r. \tag{2.30}$$

Under a ballistic approximation t_r has a quadratic form. However, if we introduce an additional far field approximation, we can determine a simpler expression for t_r. As illustrated in Figure 2-1, let $\vec{R}$ be the location of a pixel on the detector, $\vec{R}_{cm}(t_{cm})$ be the center of mass of the electron distribution, $\vec{n} = \vec{R} - \vec{R}_{cm}(t_{cm})$ and where,

$$t_{cm} = t - \frac{|\vec{R} - \vec{R}_{cm}(t_{cm})|}{c}.$$

In the limit in which the detector is far away with respect to the size of the electron distribution such that,

$$|\vec{R}_{cm}(t_{cm}) - \vec{r}_i(t_r)| \ll |\vec{R} - \vec{R}_{cm}(t_{cm})|,$$

we can use the approximation that [6],

$$\begin{aligned}\vec{x} &= |\vec{R} - \vec{r}(t_r)| \\ &\cong |\vec{R} - \vec{R}_{cm}(t_{cm})| - \left(\vec{r}_i(t_r) - \vec{R}_{cm}(t_{cm})\right) \cdot \hat{n}. \end{aligned} \tag{2.31}$$

As a result, the expression for t_r becomes,

$$\begin{aligned} t_r &= t - \frac{|\vec{x}|}{c} \\ c\,(t_r - t_{cm}) &= c\,(t - t_{cm}) - |\vec{R} - \vec{R}_{cm}(t_{cm})| + \left(\vec{r}_i(t_r) - \vec{R}_{cm}(t_{cm})\right) \cdot \hat{n} \\ (t_r - t_{cm}) &= \frac{c(t - t_{cm}) - |\vec{R} - \vec{R}_{cm}(t_{cm})| + \left(\vec{r}(t_{cm}) - \vec{R}_{cm}(t_{cm})\right) \cdot \hat{n}}{(c - \vec{v}(t_{cm}) \cdot \hat{n})}. \end{aligned}$$

From the definition of ϕ, Equation 2.27, and the above expression for $t_r - t_{cm}$, we find that the emitted radiation is given by,

$$\begin{aligned} \vec{E}_{rad} &= A \cos\left(k(ct_r + r_z(t_r)) + \delta_1\right), \\ &= A \cos\left(k\left(c(t_r - t_{cm}) + v_z(t_r - t_{cm}) + r_z(t_{cm}) + ct_{cm}\right) + \delta_1\right), \end{aligned}$$

hence,

$$\begin{aligned} \vec{E}_{rad} = A \cos\Bigg[& \frac{k(c + v_z)}{c - \vec{v} \cdot \hat{n}} \left(c(t_r - t_{cm}) - |\vec{R} - \vec{R}_{cm}(t_{cm})|\right) \\ & + \frac{k(c + v_z)}{c - \vec{v} \cdot \hat{n}} \left((\vec{r}(t_{cm}) - \vec{R}_{cm}(t_{cm})) \cdot \hat{n}\right) \\ & + k\left(ct_{cm} + r_z(t_{cm})\right) + \delta_1\Bigg], \end{aligned} \tag{2.32}$$

where,

$$A = \frac{q^2 E_0}{4\pi\epsilon_0 m} \frac{|\vec{x}|}{(c|\vec{x}| - \vec{x} \cdot \vec{v})^3} \left[\vec{x} \times ((c\hat{x} - \vec{v}) \times \vec{g})\right]. \tag{2.33}$$

From Equation 2.32 we can see that the angular-frequency of the emitted radiation is given by,

$$\omega_f = \alpha_i \omega_i, \tag{2.34}$$

where we define,

$$\alpha_i = \frac{c + \vec{v} \cdot \hat{z}}{c - \vec{v} \cdot \hat{n}}. \tag{2.35}$$

The above expression agrees with its quantum counterpart (Equation 1.1), as long as the assumed limit of classical E&M (Equation 2.1), is taken into consideration.

If we assume that the radiation scattered by an electron at each point within a laser is given by a Gaussian distribution of energies, a method for computing the radiation scattered by multiple electrons becomes immediately evident. Under this assumption, the amplitude

of the scattered radiation for the i^{th} electron is given by,

$$A_i(\omega_f) = \frac{q^2 E(t,\vec{r}_i)}{4\pi\epsilon_0 m}\frac{1}{2\alpha_i\sqrt{\pi p}}\exp\left(-\frac{(\omega_f/\alpha_i-\omega_0)^2}{4p}\right)\frac{|\vec{x}_i|}{(c|\vec{x}_i|-\vec{x}_i\cdot\vec{v}_i)^3}\left[\vec{x}_i\times((c\hat{x}_i-\vec{v}_i)\times\vec{g}_i)\right]. \tag{2.36}$$

The total electric field emitted by all of the electrons is,

$$E_{tot}(\omega_f) = \sum_i^N A_i \cos\left(\omega_f\left((t-t_{cm})-\frac{|\vec{R}-\vec{R}_{cm}(t_{cm})|}{c}\right)+\omega_i\theta_i+\delta_1\right),$$

where,

$$\theta_i = \alpha_i\left(\frac{(\vec{r}(t_{cm})-\vec{R}_{cm}(t_{cm}))}{c}\cdot\hat{n}\right)+\left(t_{cm}+\frac{r_z(t_{cm})}{c}\right). \tag{2.37}$$

Switching to complex notation,

$$\begin{aligned}E_{tot}(\omega_f) &= \sum_i^N A_i \exp\left(i\omega_f\left((t-t_{cm})-\frac{|\vec{R}-\vec{R}_{cm}(t_{cm})|}{c}\right)+i\omega_i\theta_i+i\delta_1\right)\\ &= \left[\sum_i^N A_i\exp\left(i\omega_i\theta_i+i\delta_1\right)\right]\exp\left(i\omega_f\left((t-t_{cm})-\frac{|\vec{R}-\vec{R}_{cm}(t_{cm})|}{c}\right)\right).\end{aligned}$$

As a result, the time average intensity is given by,

$$I(\omega_f) = \frac{\epsilon c}{2}|E_{tot}|^2,$$

hence,

$$I(\omega_f) = \frac{\epsilon c}{2}\left|\sum_i^N A_i\exp\left(i\omega_i\theta_i+i\delta_1\right)\right|^2. \tag{2.38}$$

Finally, the total intensity is the found by integrating over ω_f,

$$I_{tot} = \int_0^\infty I(\omega_f)d\omega_f. \tag{2.39}$$

In conclusion, we have determined a method to incorporate phase into our calculation for the emitted radiation. Equations 2.38 and 2.39 summarize the procedure used in our simulation for sampling the emitted radiation.

2.6 Ideal Electron-Electron Separation

From Equation 2.38 we can see that the i^{th} and j^{th} electrons radiate in-phase when,

$$2\pi a = \omega_i\theta_i - \omega_j\theta_j,$$

where a is an integer.

If we assume that the electrons are traveling with the same velocity vector, such that $\alpha_i = \alpha_j$, and let $\hat{n} = \hat{z}$, we find that,

$$\begin{aligned} 2\pi a &= \omega_i(\alpha_i + 1)\frac{(\vec{r}_i(t_{cm}) - \vec{r}_j(t_{cm})) \cdot \hat{n}}{c}, \\ &= \omega_i(\alpha_i + 1)\frac{\Delta z}{c}, \end{aligned}$$

hence for $a = 1$,

$$\Delta z = \frac{\lambda(c - v_z)}{2c}, \tag{2.40}$$

where λ is the wavelength of the laser. We note that this is the same ideal separation as in the non-relativistic case (Equation 1.11).

2.7 Time-Averaged Equations of Motion and Radiation Drift

To incorporate additional effects such as space-charge forces and effects due to the finite length of a laser pulse, we can determine an approximate time averaged form of the equation of motion by averaging over a period for ϕ,

$$\langle \vec{r} \rangle = \frac{1}{2\phi}\int_{\phi}^{\phi+\frac{2\pi}{k}} \vec{r} \quad d\phi,$$

and introducing a variable for the averaged ϕ, mainly $\langle \phi \rangle = \phi + \pi$.

Doing so, we find that the time average position of the particles is given by,

$$\begin{aligned} \langle x \rangle &= \frac{p_x}{c_1}\langle \phi \rangle + c_3, \\ \langle y \rangle &= \frac{c_2}{c_1}\langle \phi \rangle + c_4, \\ \langle z \rangle &= -\frac{\langle \phi \rangle}{2c_1^2}\left(m^2c^2 + p_x^2 - c_1^2 + c_2^2 + \left(\frac{qE_0}{ck}\right)^2 \frac{1}{2}\right) + c_5. \end{aligned}$$

Notice that while the time averaged expressions for x and y are independent of the laser field strength, the time average expression for z contains a term proportional to $-E_0^2$. This term, results in a time averaged drift of the electron in the direction of $\hat{k}$ as the electron is exposed to the laser field.

Likewise, the expressions for the time averaged momentum of the electron are given by,

$$\begin{aligned} \langle p_x \rangle &= \frac{p_{x0}}{c_1}, \\ \langle p_y \rangle &= \frac{c_2}{c_1}, \\ \langle p_z \rangle &= -\frac{1}{2c_1^2}\left(m^2c^2 + p_x^2 - c_1^2 + c_2^2 + \left(\frac{qE_0}{ck}\right)^2 \frac{1}{2}\right). \end{aligned}$$

2.8 Space-Charge effects

Due to the relativistic motion of the electrons, the static Coulomb force,

$$\vec{F}_{ij} = \frac{q_i q_j}{4\pi\epsilon_0} \frac{\vec{r}_{ij}}{|\vec{r}_{ij}|^3},$$

is only valid in the rest frame of the electron distribution. However, as a result of the non-simultaneity of special-relativity, computing the repulsion forces in the rest frame would complicate the integration of the motion of each electron in the lab frame due to the fact that, the static Coulomb forces experienced by each electron at a given moment in time in the rest frame, are experienced by the electrons in the lab frame at different times.

As a result, we decided to use a different approach by using Equation 2.20 in conjunction with a ballistic approximation to determine the force on a given electron in the lab frame based on the current position of the other electrons.

From Equation 2.20, we find that the force on electron i by electron j is given by,

$$\vec{F}_{ij} = q_i \left(\vec{E}_j(\vec{r}_i) + \vec{v}_i \times \vec{B}_j(\vec{r}_i) \right).$$

Using,

$$B_j = \frac{1}{c} \hat{x}_{ij} \times \vec{E}_j,$$

we find that,

$$\vec{F}_{ij} = \frac{q_i q_j}{4\pi\epsilon_0} \frac{|\vec{x}_{ij}|}{(\vec{x}_{ij} \cdot \vec{u}_{ij})^3} \left[\left((c^2 - v_j^2)\vec{u}_{ij} \right) + \frac{\vec{v}_i}{c} \left(\hat{x}_{ij} \times \left((c^2 - v_j^2)\vec{u}_{ij} \right) \right) \right], \tag{2.41}$$

where,

$$\begin{aligned} \vec{x}_{ij} &= \vec{r}_i(t) - \vec{r}_j(t_r), \\ \vec{u}_{ij} &= c\hat{x}_{ij} - \vec{v}_j, \\ t_r &= t_0 - \frac{|\vec{x}_{ij}|}{c}, \end{aligned}$$

and where t_0 is the current time. Using the ballistic approximation on electron j that,

$$\vec{r}_j(t_r) = (t_r - t_0)\vec{v}_j + \vec{r}_j(t_0),$$

Equation 2.41 can be easily computed. The total force on electron i can then be determined by summing over all of the other electrons,

$$\vec{F}_i = \sum_{j \neq i} \vec{F}_{ij}. \tag{2.42}$$

To simplify implementation, we can assume to good approximation that the electrons are effectively at rest with respect to each other in the sense that,

$$\vec{v}_i = \vec{v}_j.$$

We note that under this approximation, our method for computing space-charge forces is

equivalent to computing the forces in the rest frame using the static Coulomb force and then transforming into the lab frame.

Chapter 3

Numerical Methods for ICSSim

This chapter discusses various numerical algorithms used in the code written as part of this thesis.

3.1 Integration of Time-Average Motion

To calculate the trajectory of the electrons, it is necessary to integrate the equations,

$$\frac{d\vec{p}_i}{dt} = \vec{F}_i(\vec{x}),$$
$$\frac{d\vec{x}_i}{dt} = \frac{\vec{p}_i}{\gamma m_i},$$

where $F(\vec{x})_i$ is given by Equation 2.42. Using the relation that,

$$\gamma = \sqrt{\left(\frac{p}{mc}\right)^2 + 1}$$

we find that,

$$\frac{d\vec{p}_i}{dt} = \vec{F}_i(\vec{x}_i),$$
$$\frac{d\vec{x}_i}{dt} = \frac{\vec{p}_i}{\sqrt{\left(\frac{p_i}{c}\right)^2 + m_i^2}}.$$

As a result, we use a modified form of the leapfrog integration technique [2], accurate to second order. At a given time step t, the position and momentum of each electron are updated according to,

$$\vec{x}_i(t) = \vec{x}_i(t - \Delta t) + \frac{\vec{p}_i(t - \Delta t/2)c}{\sqrt{p_i(t - \Delta t/2)^2 + m_i^2 c^2}}\Delta t,$$
$$\vec{p}_i(t + \Delta t/2) = \vec{p}_i(t - \Delta t/2) + \vec{F}_i(\vec{x}_i(t))\Delta t,$$

where Δt is the stepping size.

3.2 Calculation of Space-Charge Effect using Octree

For a large number of particles ($\sim 10^6$), determining the space-charge force by using Equation 2.42 directly is computationally intensive. However, we note that since the space-charge force has essentially a $1/r^2$ dependence, the largest contributions are provided by neighboring electrons, where as groups of electrons located at distances larger than their characteristic size can be approximated by a single charge at the center of the group. As a result we can accelerate space-charge calculations by using an Octree structure to cluster distant macroparticles in a similar manner as in the Barnes-Hut algorithm [1].

The acceleration algorithm proceeds as follows. At each time step, the list of electrons is first traversed to determine the average velocity, and the center and size of the distribution. Next, an Octree is generated covering the space of the electron distribution. The Octree begins with a root node, corresponding to the entire space. When an electron is added to a node, the node uses the electron's total charge and position to keep track of the center of mass and total charge of all of the electrons ever added to it. Next the node checks whether an electron is already assigned to it. If not, the electron is assigned to the node. If so, the node subdivides its space into eight sections, creating one new child-node for each of the eight subsections, and then adds the electron assigned to it and the newly added electron to the respective child-node based on which subsection they reside in, initiating a similar process for the child-nodes. The end result is a tree structure where each node is either assigned to an electron, or contains the center of mass and total charge of the electrons residing within a certain subsection of the total space.

To compute the space-charge force on an electron, the Octree is traversed starting from the root node. For each child-node within the tree we check whether,

$$\frac{w_n}{x_{ni}} < \xi, \tag{3.1}$$

where w_n is the width of the space the node represents, x_{ni} is the distance from the electron to the node in the rest frame of the distribution and ξ is a variable parameter (by default $\xi = 0.5$). If the above condition is met, then the total charge and center of mass of the node is used to approximated the sum of the forces from the electrons stored underneath it. If not, then the process is repeated for all of the child-nodes, until either a node meets the sufficient criteria or a node which is assigned to an electron is found. We can see that in the limit that $\xi = 0.0$ the algorithm is equivalent to simply computing the direct sum.

3.3 Simulation Overview

We now provide an overview of the simulation routine. The simulation is conducted entirely in the lab reference frame, with the electrons traveling along the $\hat{z}$ direction and the laser pulse along the $-\hat{z}$ direction. The electron distribution is represented within the simulation by a number of macro-particles ($\sim 10^6$), each with a potentially varying mass and charge.

At the start of the simulation, the laser pulse is positioned in a state such that after a given time t_{2f} it reaches its focus at the origin of the coordinate system. Likewise, letting v_z be the average velocity of the electron distribution along the z-axis, the center of mass of the electron distribution is positioned at a distance $z_0 = -v_z t_{2f}$. As a result, after a given time t_{2f} both the center of the laser and the center of the electron distribution overlap at the origin of the coordinate system. Finally a detector is located a given distance R_0 along

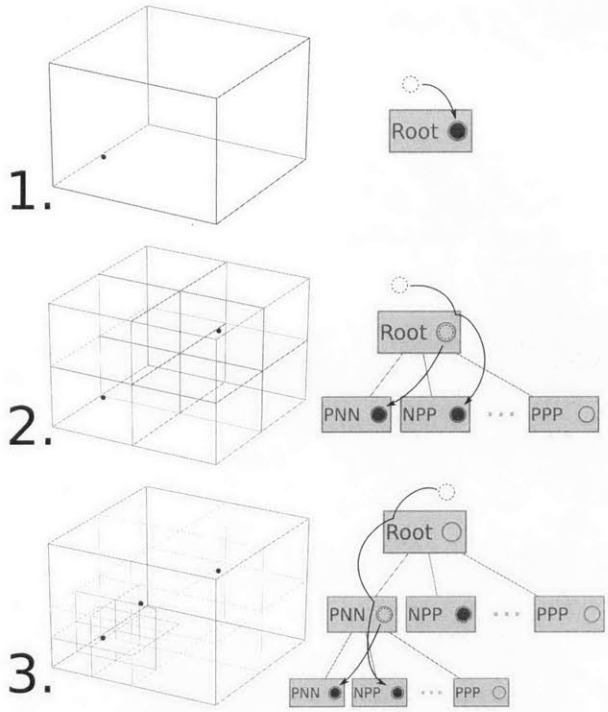

Figure 3-1: Illustration of the space subdivisions (left) and node tree (right) for the generation of an Octree with three electrons. In the first step, the first electron is added to the root node. When the second electron is added (step 2), the space of the root node is subdivided into eight subsections and, the root node adds both electrons to the node representing the respective subsection it is in. Each node in the tree carries out a similar process as is illustrated in step 3 when the third electron is added.

the $\hat{z}$ direction and is given a specific time t_d at which to sample the radiation. For most applications, we would like to sample the radiation emitted when the center of the laser and electron distribution overlap. Hence,

$$t_d = t_{2f} + \frac{R_0}{c}.$$

The routine proceeds as follows. First, the retarded sample time of the center of mass is computed using,

$$t_{cm} = t_d - \frac{|R_0\hat{z} - R_{cm}(t_{cm})|}{c}.$$

Next the equations of motion are integrated according to the method described in Section 3.1 until the time t_{cm} is reach. Once this time has been reached, the radiation observed by the detector is sampled using the new values for the velocity and positions of the electrons with the procedure established in Section 2.5. To compute Equation 2.39, the integral over w_f is numerically approximated by sampling discrete values for w_f, according to,

$$\begin{aligned} I_{tot} &= \int_0^\infty I(\omega_f) d\omega_f, \\ &\cong \sum_{n=0}^{N} I\left(\omega_{fc} + \left(\frac{n}{N} - \frac{1}{2}\right)\Delta\omega_f\right), \end{aligned}$$

where both the center of the sampled distribution ω_{fc} and $\Delta\omega_f$ are specified parameters.

Chapter 4

Analysis of an Example ICS Source

Using the simulation routine we have just described, we will now analyze the radiation produced by an example ICS source using both a coherent and incoherent electron distribution. The parameters for our example ICS source are listed in Table 4.1.

4.1 Initial Electron Distribution

Figure 4-1 illustrates the square density modulation we have used for the initial spatial distribution of the electrons within our simulations. This density modulation is characterized by the period of the distribution λ_b, the fill-factor f_f, the total number of microbunches N, the x and y RMS size and the total charge within the pulse. The distribution is created by first evenly distributing the total charge between all of the macroparticles and then randomly assigned each macroparticle to a microbunch within the pulse. The macroparticles within each microbunch are then arranged along the z-axis within the space described by the fill-factor according to a uniform distribution, while being arranged along the x and y axis according to the Gaussian distribution described by the respective rms parameter. Figures 4-2 and 4-3 plot the x,y and z profiles of the initial macroparticle distribution generated by this method.

While our implemented simulation routine is capable of handling a different velocity for each macroparticle, in the simulations below we have decided to give each macroparticle the

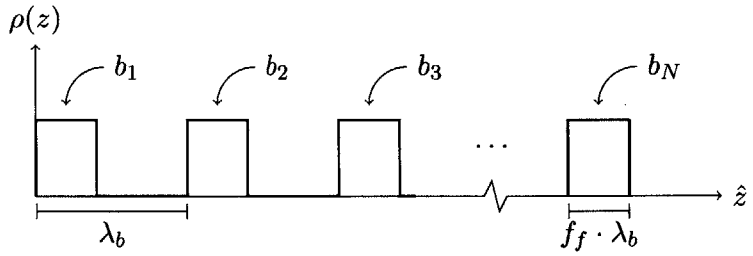

Figure 4-1: Illustration of the square density used for the initial distribution of the electrons along with the parameters used in the text. Note that within each period of the beam, the electrons occupy a region given by the product of the fill-fraction f_f and the period of the density λ_b. Note that in the case the fill factor $f_f = 1.0$, the macroparticles are uniformly distributed along the z axis.

Electron Pulse Parameters	
Microbunches	400
Macroparticles	10^6
Kinetic Energy	2×10^6 eV
Total Charge	-1.60218×10^{-13} C
Period	1.04630×10^{-8} m
Fill Factor	0.5
x rms size	10^{-6} m
y rms size	10^{-6} m
Laser Pulse Parameters	
Pulse Type	Gaussian Plane-Wave
Peak Electric Field	3×10^6 N/C
Wavelength	10^{-6} m
Pulse Length	1.25×10^{-4} m
Detector Parameters	
Distance from origin	1 m
Time at which to Sample	3.33605×10^{-9} s

Table 4.1: Parameters for an example ICS source. To simulate the output from a similar incoherent source, we simply set the fill-factor to 1.0, resulting in a uniform distribution along the $\hat{z}$ direction.

same velocity to more easily study effects due to the bunch separation. The velocity of the macroparticles is related to the kinetic energy of a single electron within the distribution according to,

$$\vec{v} = c\frac{\sqrt{\left(\frac{E_k}{mc^2}+1\right)^2 - 1}}{\frac{E_k}{mc^2}+1}\hat{z},$$

where mc^2 is the rest energy of a single electron. Likewise, simulations presented in this section have been computed without space-charge effects.

4.2 Determining Optimal Electron Bunch Separation

Figure 4-4 compares the output intensity as a function of the period of the electron distribution λ_b for both the coherent ($f_f = 0.5$) and incoherent ($f_f = 1.0$) case. We note that the period corresponding to the peak intensity for the coherent simulation results agrees quite well with the theoretical ideal period of $1.04630 \times 10^{-8}m$ given by Equation 2.40. In comparison, a scan of the incoherent case shows no strong variations in intensity, as expected. We can likewise see that in the limit far from the ideal period, both the coherent and incoherent distributions produce roughly the same intensity, while the ratio of coherent to incoherent intensity close to the ideal period is $\approx 10^5$, as expected when the emitted fields add in-phase as compared to with uncorrelated-phases.

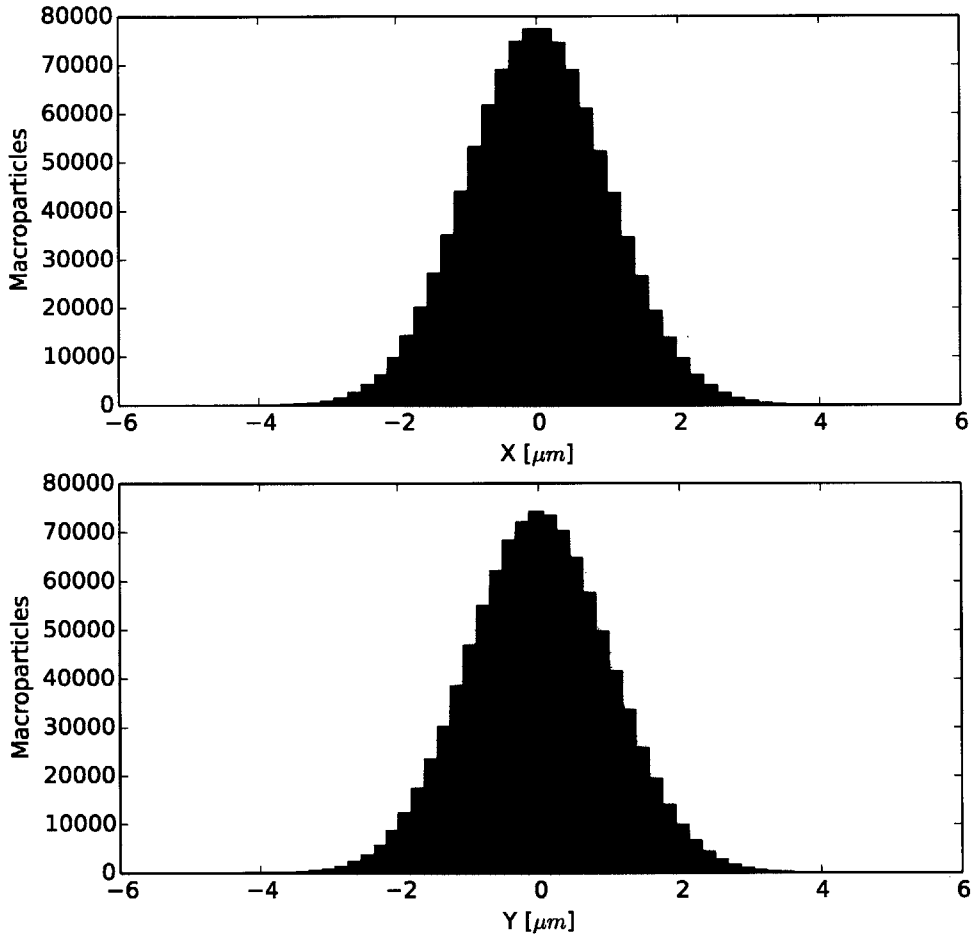

Figure 4-2: Initial distribution of simulation macroparticles in the X and Y direction. In total 10^6 macroparticles were used in the simulation.

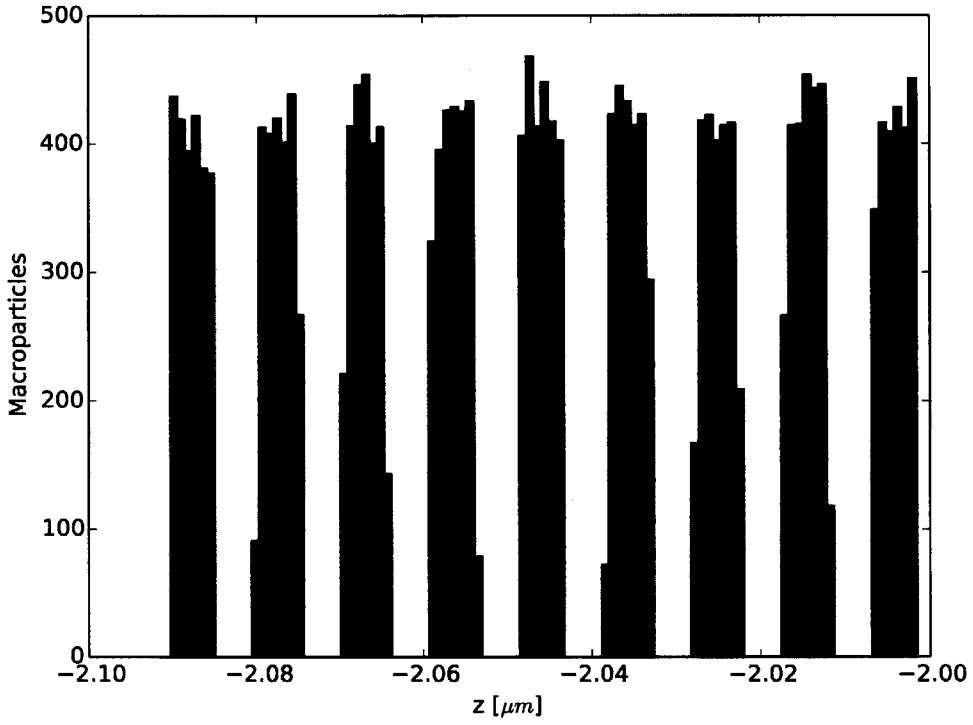

Figure 4-3: The last nine microbunches in the initial electron distribution to visualize the average distribution of macroparticles within a microbunch. The total distribution contains 400 of such microbunches.

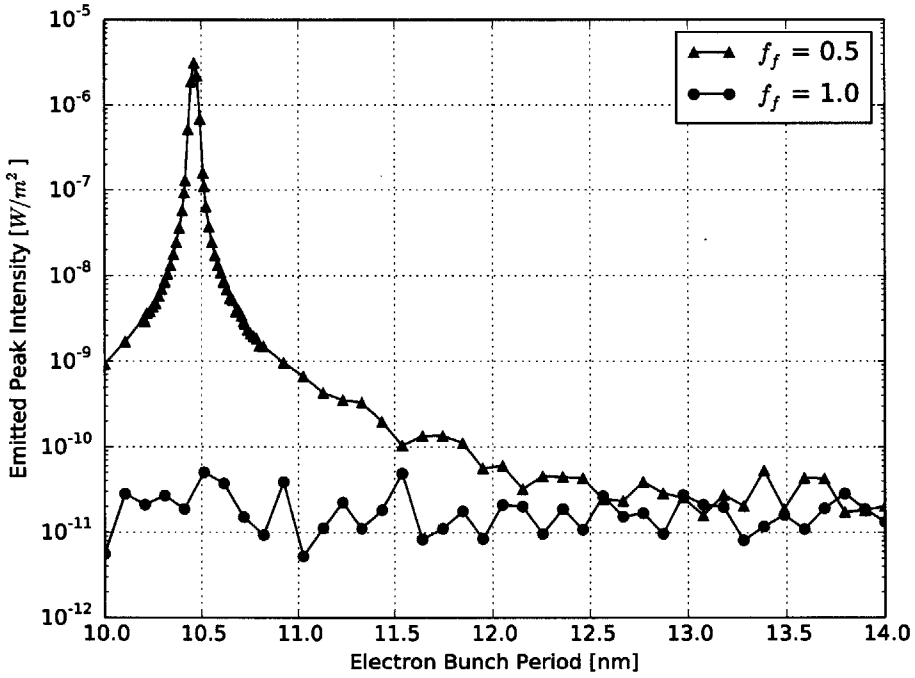

Figure 4-4: Comparison of the output intensity as a function of the period of the electron distribution λ_b for both a coherent ($f_f = 0.5$) and incoherent ($f_f = 1.0$) case.

4.3 Resulting Radiation Profile

Using the ideal period ($\lambda_b = 1.04630 \times 10^{-8} m$), we proceed to compute the spatial intensity profile of the beam for both the incoherent and coherent case. Figure 4-5 plots the spatial intensity profile of the output beam while Figure 4-6 plots the spatial profile of the average radiated energy for the coherent $f_f = 0.5$ case. We can see that the peak radiated intensity is around $1.2e6\ W/m^2$. For comparison, Figure 4-7 plots the intensity for the incoherent $f_f = 1.0$ case. From the two profiles we can see that the intensity from the coherent electron distribution is around five orders of magnitude larger than that from the incoherent distribution.

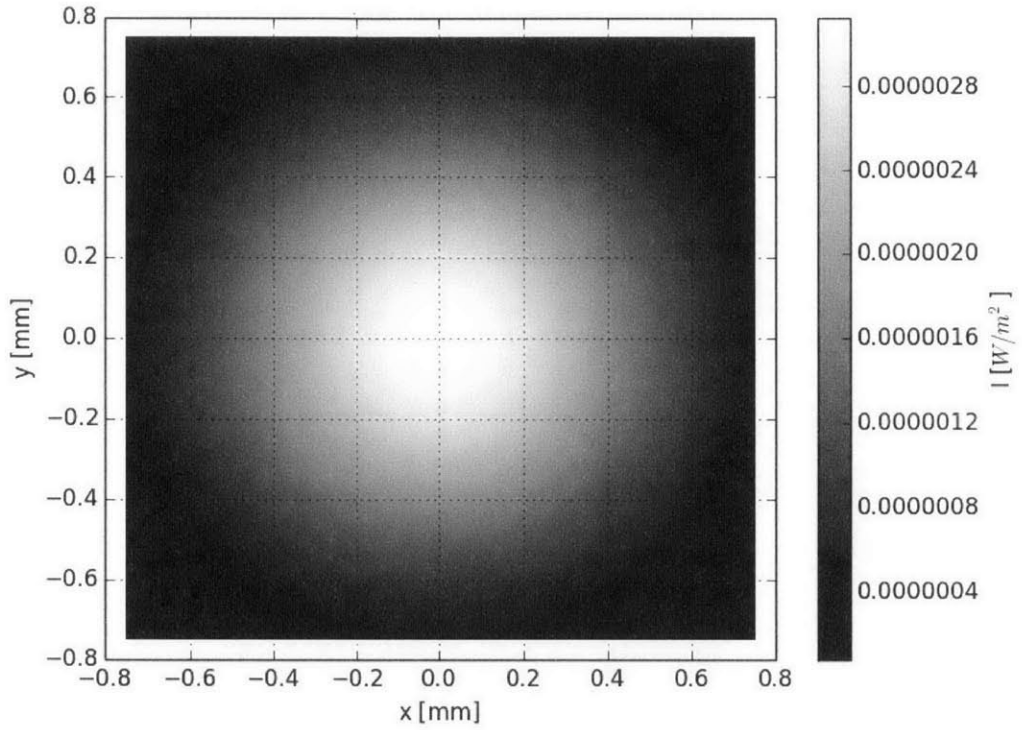

Figure 4-5: Emitted intensity profile for the example ICS source parameters for a fill-factor of $f_f = 0.5$ representing a coherent ICS source. We can see that the peak intensity is around $2.9e-6\ W/m^2$.

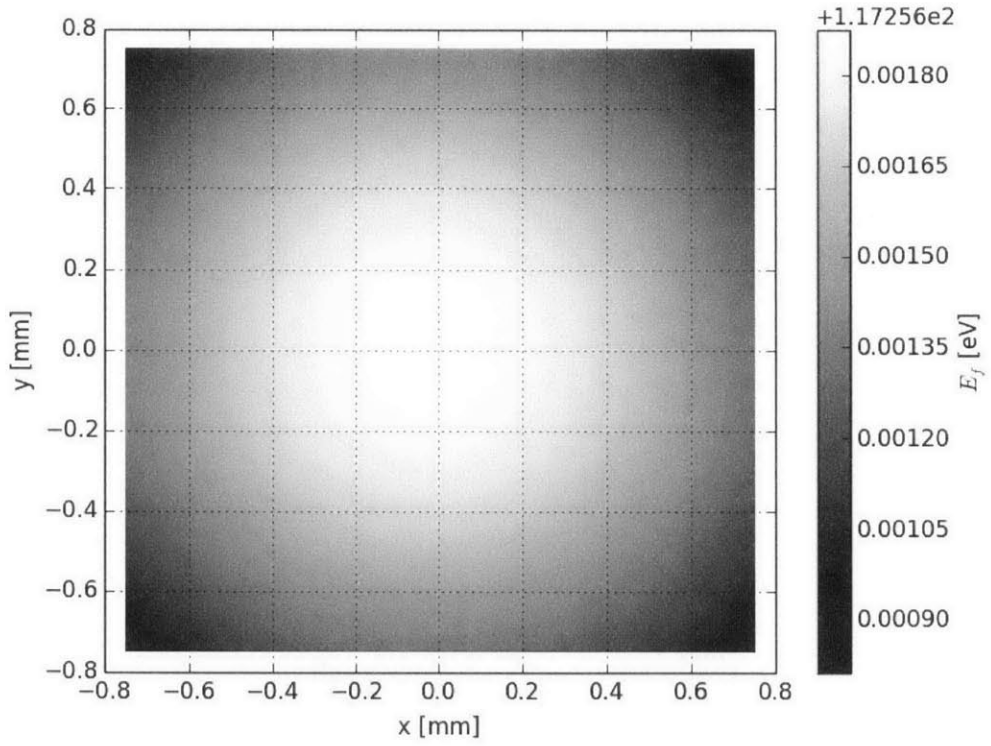

Figure 4-6: Spacial distribution of the average radiated energy for a fill-factor of $f_f = 0.5$, representing a coherent ICS source.

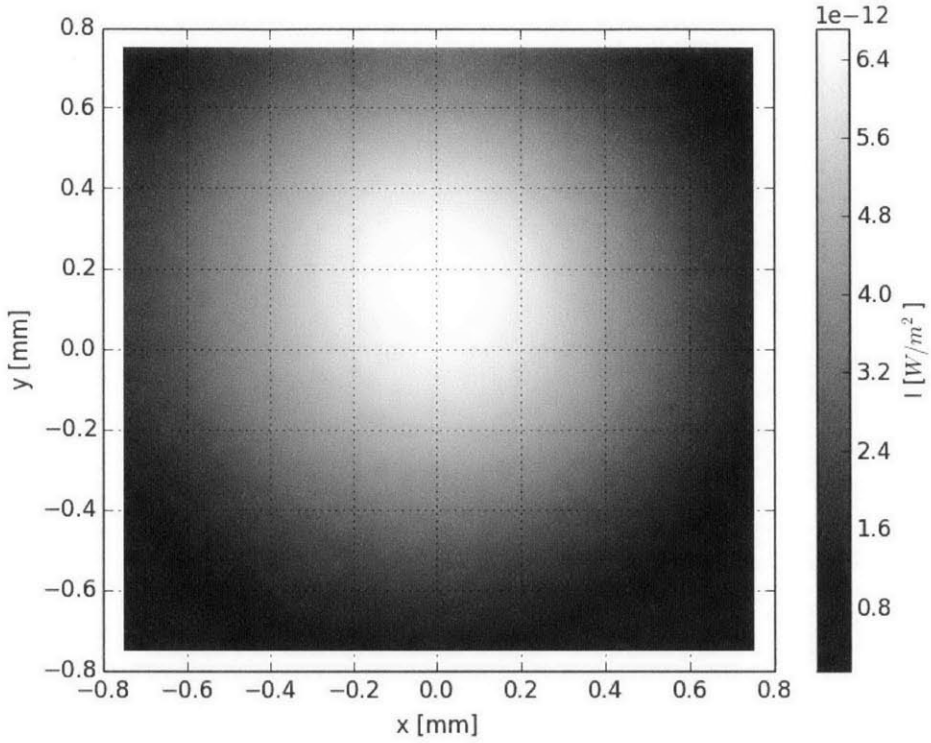

Figure 4-7: Emitted intensity profile for the example ICS source parameters with a fill-factor of $f_f = 1.0$ representing a comparable incoherent ICS source. Do to the low intensity, statistical fluctuations within the distribution of the 10^6 macroparticles are sufficient to visibly alter the computed profile of the beam. We can see that as a result of these fluctuations, the peak intensity is slightly off center.

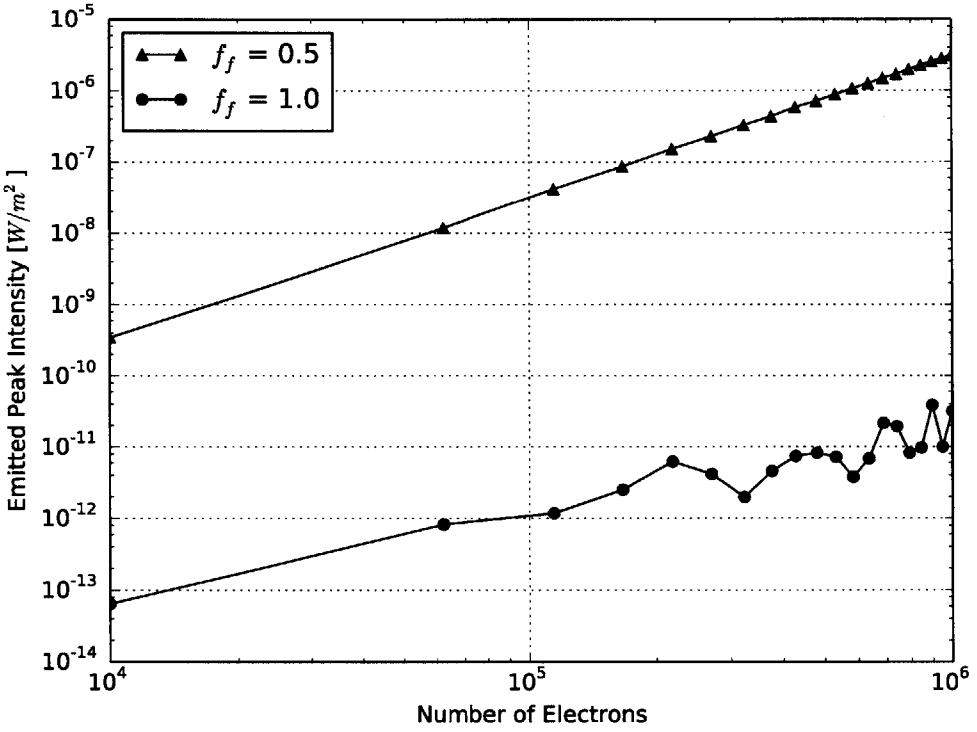

Figure 4-8: Emitted peak intensity as a function of the number of electrons within the beam for both the coherent $f_f = 0.5$ and incoherent $f_f = 1.0$ case. As expected, while the incoherent case scales like the total number of electrons within the beam, the incoherent case scales like the square of the total number of electrons.

Chapter 5

Conclusion

We have determined a method for incorporating both space-charge and phase effects into the calculations of the radiation scattered during ICS and have implemented and used this method to simulate the output characteristics for an example ICS source.

Likewise, we have used our simulation routine to identify the ideal electron distribution period and have provided a comparison between the radiation emitted by a incoherent and coherent electron distributions.

We conclude by summarizing the main approximations of our described technique. First, space-charge calculations require that the electrons be traveling at a similar enough speed such that the static Coulomb force is valid in the rest frame of the electron distribution. Secondly, our method for sampling the scattered radiation requires that the strength of the electric field of the laser is weak such that, in comparison to the total momentum of the electron,

$$\frac{qE_0}{ck} \ll |\vec{p}|.$$

Finally, our radiation sampling method requires that the electron distribution, at the time of the radiation sampling, has a total length much smaller than the distance between the distribution's center of mass and the detector.

We hope that the software and routine developed as part of this thesis will be useful in the study and design of future ICS sources which take advantage of in-phase super-radiant emission and, ultimately, in enabling for hard x-ray beams to become more accessible to research and industry.

Bibliography

[1] J. Barnes and P. Hut. A hierarchical O(N log N) force-calculation algorithm. *Nature*, 324:446–449, December 1986.

[2] J.P. Boris. Relativistic plasma simulation-optimization of a hybrid code. In *Proceedings of the Fourth Conference on Numerical Simulation of Plasma*, pages 3–67, Washington DC, November 1970. Naval Res. Lab.

[3] W. S. Graves, F. X. Kärtner, D. E. Moncton, and P. Piot. Intense superradiant x rays from a compact source using a nanocathode array and emittance exchange. *Phys. Rev. Lett.*, 108:263904, Jun 2012.

[4] D.J. Griffiths. *Introduction to electrodynamics.* Prentice Hall, 1999.

[5] Keith Hagenbuch. Free electron motion in a plane electromagnetic wave. *American Journal of Physics*, 45(8), 1977.

[6] L.D. Landau and .. . *The Classical Theory of Fields.* Number v. 2 in Course of theoretical physics. Butterworth Heinemann, 1975.

[7] E. S. Sarachik and G. T. Schappert. Classical theory of the scattering of intense laser radiation by free electrons. *Phys. Rev. D*, 1:2738–2753, May 1970.

[8] Julian Schwinger. On the classical radiation of accelerated electrons. *Phys. Rev.*, 75:1912–1925, Jun 1949.

[9] A.E. Siegman. *Lasers.* University Science Books, 1986.

[10] Zhongyang Wang, Zhengquan Zhang, Zhizhan Xu, and Qiang Lin. Space-time profiles of an ultrashort pulsed gaussian beam. *Quantum Electronics, IEEE Journal of*, 33(4):566–573, Apr 1997.

[11] Richard W. Ziolkowski and Justin B. Judkins. Propagation characteristics of ultrawide-bandwidth pulsed gaussian beams. *J. Opt. Soc. Am. A*, 9(11):2021–2030, Nov 1992.